Chemical Science

Accepted Manuscript

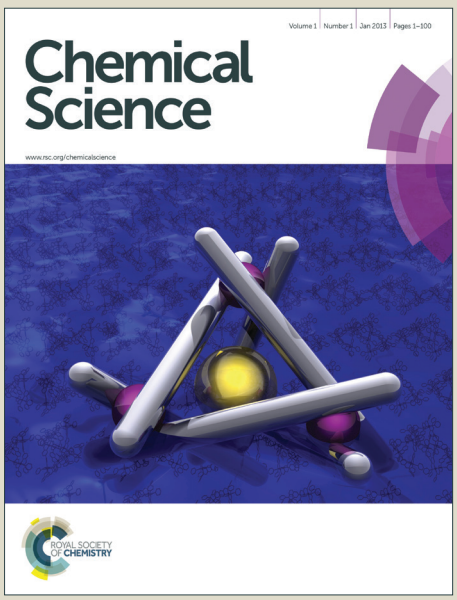

ROYAL SOCIETY OF CHEMISTRY

www.rsc.org/chemicalscience

Cite this: DOI: 10.1039/c0xx00000x

www.rsc.org/xxxxxx

ARTICLE TYPE

Millisecond lifetime imaging with europium complex using a commercial confocal microscope under one or two-photon excitations

Alexei Grichine,[a,b,c*] Alexandre Haefele,[d] Simon Pascal,[d] Alain Duperray,[a,b,c] Richard Michel,[e] Chantal Andraud,[d] Olivier Maury[d*]

Received (in XXX, XXX) Xth XXXXXXXXX 20XX, Accepted Xth XXXXXXXXX 20XX
DOI: 10.1039/b000000x

The long luminescence lifetime of lanthanide based bioprobes is a great advantage for their specific detection in autofluorescent or labelled cells and tissues. It is also a valuable tool for sensing the physico-chemical microenvironment and molecular interactions by Förster resonance energy transfer (FRET). However, standard confocal and multiphoton laser scanning microscopes are not adapted for imaging with such temporal resolution because the typical pixel dwell time is too short compared to the luminescence lifetime. We show that the rapid sampling rate and laser control of the usual confocal microscope can instead be used for precise measurement of the long lifetime decays (µs to ms range). Furthermore, both raster- and line-scanning microscopes can specifically detect long luminescence signal in time-gated mode by shifting the pinhole or the confocal slit in lagging direction. We characterized the subcellular localization and accurately measured the millisecond luminescence lifetimes of the benchmark two-photon europium probe $[Na]_3[Eu\mathbf{L}^{1G}{}_3]$ and specifically imaged this label in the presence of short living fluorescent species. Fine variations of the luminescence lifetime of this lanthanide complex were revealed and mapped in cells in the presence of a FRET acceptor, allowing quantification of the FRET efficiency independently of donor concentration. These results demonstrate high and yet unexploited potential of the quantitative confocal and multiphoton microscopy for the time-gated and lifetime imaging of lanthanide-based biological sensors.

Introduction

f-block elements, such as Tb(III), Eu(III) or Yb(III), constitute the increasingly popular basis for the synthesis of Lanthanide Luminescent Bio-probes (LLB) since their unique photophysical properties[1-2] (sharp emission from the visible to the red or the NIR, large (pseudo)-Stokes shift, long lifetime) make them particularly attractive for *in-vivo* imaging.[3-5] Furthermore, the recent development of conjugated organic antennae exhibiting charge transfer transitions has allowed their sensitization by nonlinear two-photon (2P) excitation process with large 2P cross-section (σ^2).[6-11] These results open the way for the design of 2P-LLB combining the intrinsic advantages of rare earth spectroscopy and those of 2P microscopy[12] (NIR excitation, 3D resolution…) and many examples of cellular[13-20] and thick tissue[21] imaging have been reported in the literature.

Moreover, the particularly long luminescence lifetime of lanthanides (µs-ms) allows the time-resolved or time-gated (TG) imaging with high contrast due to the extinction of the short-living signals[22-26] (e.g. autofluorescence background (ps), fluorescent organic probes or proteins (ns)). In addition, a careful ligand engineering enables the design of complexes whose luminescence response (spectral shape, quantum yield and lifetime is sensitive to the local microenvironment, to the presence of oxygen or various substrates (pH, metal ions, bicarbonate, lactate, urate).[27-31] Finally, bright LLBs allow the detection of molecular interactions by Förster Resonance Energy Transfer (FRET)[32] in applications like fluorescence immunoassays,[33-34] DNA hybridization or cell activity assays.[35-38] The TG-imaging is based on the pulsed excitation and the delayed detection of the luminescence. It is a firmly established technique in spectroscopic analysis and in wide-field microscopy, albeit often using custom developed TG-microscopes.[39-42]

In this field, long-standing and recent breakthrough developments are carried out by the groups of Piper, Yin and co-workers.[43] On one hand, an original orthogonal scanning (OSAM) approach allowed dramatic acceleration of the TG-imaging long lifetime probes in analytical applications such as rare events screening.[44] On the other hand, a new concept of lanthanide-doped nanocrystals with precise and adjustable luminescence lifetimes (τ-Dots) allows temporally and spectrally multiplexed imaging.[45] The reported luminescence lifetimes of Tm:Yb upconversion τ-Dots are of tens to hundreds µs and are measured with the purpose-build laser scanning microscope.

However, the gated and delayed detection of the luminescence signal yields only the integrated intensity within a certain decay range. Importantly, it does not allow the uncoupling of the initial amplitude and the characteristic decay time. These two complementary parameters are related to the probe concentration

and its physico-chemical microenvironment (hydration number, energy transfer, quenchers, pH, etc.) most of which are often unknown in biological media, and differently affect the total luminescence signal. The precise analysis of the lifetime decay shape can report on subtle changes in probe state, the presence of different probe populations, the molecular complexes formation and the ratio of interacting *vs.* non-interacting molecules, regardless the variations of the probe concentration or the aberrations in the optical path *in situ*.

Various methods of Lifetime Imaging Microscopy (LIM) were developed in the past decades for *nanosecond* fluorescent probes, based on time-gating, time correlated single photon counting, or phase modulation.[46-47] They are now widely applied to fluorescent proteins, cell organelle probes or immuno-labels as well as to the characterization of tissue autofluorescence. However, the lifetime measurements and imaging in *micro-* to *millisecond* time-scale under the microscope remain much less common. Recently, the long-lifetime imaging methods were reported by using the multiple frequency phase modulation in the wide field microscopy[48-49] or the time-correlated single photon counting in the laser scanning 2P microscopy.[50] These advances are possible due to the instrumental improvements of the intensified CCDs and the pulsed laser control but they stay technically challenging, rather costly and require substantial modifications of the microscope configuration. A commercially available phase modulation system for the long lifetimes (LIFA-X, Lambert Instruments) still suffers from a limited lifetime range (< 1 ms), low photon efficiency (*i.e.* the ratio of used photons to all detectable photons) and a poor precision in case of multi-exponential decays. Up to 16 successive images are necessary to calculate a single-exponential lifetime image.

The temporal resolution of a standard confocal microscope, however, can also be exploited for such long-lifetime measurements. Indeed, conventional laser scanning microscopes feature the pixel sampling time and laser excitation control in µs to ms range, which are well-tailored for the time domain measurements of LLB decays. The first implementation of the time domain decay sampling using a confocal microscope was proposed as early as 1992 by Buurman*et al*.[51] This microscope was modified with a 25-MHz electro-optical chopper and TG-detection in two or more temporal windows and allowed ns resolution. Pulsed lasers used in modern confocal microscopes, such as DPSS or Ti:Sa generally function at MHz repetition rate resulting in detection window of only tens of ns. For the longer lifetimes Beeby *et al*.[26] reported the use of a cavity-dumped mode locked Ti:Sa laser to reduce the pulse frequency down to 1.8 MHz allowing a time-gating experiment of 480 ns duration with a very short delay of 75 ns from the laser pulse. This method was successfully applied to spectroscopic time resolved measurements. The similar laser modification was reported very recently in multiphoton time-resolved microscopy by Williams, Weinstein and co-workers. for the imaging of µs-lifetime cyclometallated platinum(II) complex.[52]

Here we demonstrate that a standard *usual* 1P confocal or 2P laser scanning microscope can be used for the simple and precise luminescence lifetime measurements in µs-ms range using the AOTF (acousto-optical tunable filter) shaping of the excitation pulse and continuous sampling of the lifetime decay in each pixel, a technique that we call Temporal Sampling Lifetime Imaging Microscopy (TSLIM). It should be stressed, that unlike TG-imaging or multiple frequency phase modulation, TSLIM uses most of detected photons, thus minimizing photobleaching and maximizing the photon efficiency. However, the high precision of luminescence decays is obtained at the expense of the overall acquisition time, which is in the order of minutes.

In this regard TSLIM is complementary to the much faster but less precise Pinhole Shifting Lifetime Imaging Microscopy (PSLIM).[53] This original approach for the long-lifetime imaging was also developed using the *usual* commercial confocal microscope. It allowed selective detection of the long-living species due to the lagging of the pinhole position of few airy units (AU) back with respect to the incident rasting spot. In PSLIM, 1AU represents the time necessary to scan the number of pixels corresponding to the size of 1 Airy disk. Thus, for a given scanning speed and a pixel size, PSLIM concept is similar to the TG-imaging. It suffers however from the lack of precision of the decay curve, since only few experimental points can be obtained with different pinhole lags. The presence of the pinhole is mandatory even with 2P excitation, thus limiting the detection of non-ballistic photons and each pinhole lag should be measured as a separate image that hampers applications to mobile samples. Moreover, temporal detection window is defined by the exact size, shape and position of the pinhole and the scanning speed, which finally determine the photon efficiency and the precision of the calculated lifetime values.

Here we successfully applied both TSLIM and PSLIM under 1 or 2P excitations to cell imaging of Europium based 2P-LLB. Furthermore we extended the scope of PSLIM to the faster line-scanning confocal microscopy (LSM7 LIVE, Zeiss) opening a way to the rapid 3D TG-imaging *in vivo*. Taken together, PSLIM and TSLIM constitute a complete and complementary package for both fast specific imaging and precise measurements of the long lifetimes (that could be luminescence, delayed fluorescence or phosphorescence) using usual commercial confocal microscope working under classical 1P or nonlinear 2P excitations. These methods were illustrated by the study of the intracellular luminescent lifetimes of our benchmark europium complex for biphotonic imaging experiments, $[Na]_3[Eu\mathbf{L}^{\mathbf{1G}}_3]$[13] in fixed and living cells and in the presence of an original FRET acceptor, (**2a,b**) belonging to the heptamethine family (Fig. 1).

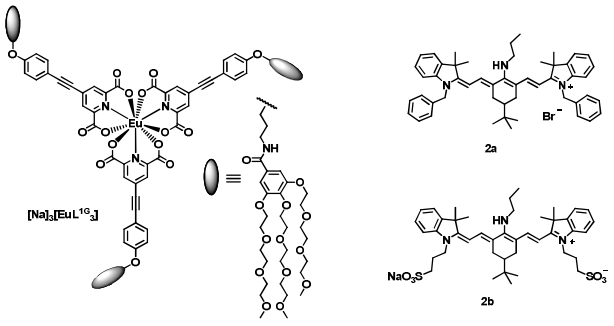

Fig. 1 Structures of europium complex and heptamethine derivatives

Results and Discussion

Photophysical properties of the probes

The $[Na]_3[Eu\mathbf{L}^{1G}_3]$ complex (Fig. 1), whose synthesis was previously described,[13] is composed of three ligands $\mathbf{L}^{1G}$ featuring a 2,6-pyridine dicarboxylic chelating part, substituted in *para* position by a conjugated 2P antenna *i.e.* the alkoxy phenyl-ethynylene fragment. The aqueous solubility of the complex is ensured by the three -$(O\text{-}CH_2CH_2)_3OMe$ fragments. It presents excellent photophysical properties both in water and organic solvents (Tab. 1). In particular, its high extinction coefficient (ε =78000 $L.mol^{-1}.cm^{-1}$ at 336 nm) combined with a quantum yield of 0.15 afforded a remarkable one photon brightness $\mathcal{B}^{(1)}$ = 11700 $L.mol^{-1}.cm^{-1}$ in water. The broadness of the absorption band makes possible the 1P luminescence excitation at 337 (ε = 78000 $L.mol^{-1}.cm^{-1}$), 365 (ε = 36000 $L.mol^{-1}.cm^{-1}$) but also at 405 nm (ε = 7000 $L.mol^{-1}.cm^{-1}$) (Fig. S1), corresponding respectively to N_2 laser, HBO mercury lamp or DPSS laser widely used in biological imaging applications. It is worth noting that this high brightness is not obtained by the optimization of the quantum yield as generally reported in the literature but rather by the increase of the absorption at the wavelength of interest. This strategy has been successfully used for the preparation of very bright europium complexes by anchoring these antennae to triazacyclononane macrocycle.[54-56] Furthermore $[Na]_3[Eu\mathbf{L}^{1G}_3]$ exhibits significant 2P cross-section ($\sigma^{(2)}$ = 92 GM at 700 nm) due to the presence of extended donor-π-conjugated system resulting in a reasonable 2P brightness in water $\mathcal{B}^{(2)}$ = 14 GM at this wavelength. The luminescence decay in water is mono-exponential with a millisecond lifetime (1.6 ms in dichloromethane), far longer than that of organic or endogenous chromophores (few ns) making this complex suitable for the time-resolved experiments *e.g.* one- or two-photon TG-imaging, or FRET. On the other hand, this complex presents moderate stability in water, explaining the lower quantum yield and lifetime compared to dichloromethane (Table. 1). As already reported for the non-functionalized $[EuDPA_3]^{3-}$ complex,[57] $[Na]_3[Eu\mathbf{L}^{1G}_3]$ partially dissociates at low concentration (about 30% at 10-50µM).

Table 1 Photophysical properties of the probes in water and organic solvents at room temperature

	λ^{abs} / nm	ε / $L.mol^{-1}.cm^{-1}$	λ^{em} / nm	ϕ / %	τ / s	σ_2 at700nm / GM
$[Na]_3[Eu\mathbf{L}^{1G}_3]$						
H_2O	336	78500	615	16[a]	1.06 x10^{-3}	96
CH_2Cl_2	330	65000	615	33[a]	1.62 x10^{-3}	92
2a						
CH_2Cl_2	652	102000	764	26[b]	1.1 x10^{-9}	
CH_3OH	617	96000	759	20[b]	0.9 x10^{-9}	
2b						
CH_3OH	623	68000	759	18[b]	0.7 x10^{-9}	
H_2O	605	49000	764	6[b]	<0.4 x10^{-9}	

[a]Quinine sulfate as reference (Φ = 54.6% in 1N sulfuric acid);[b]Cresyl Violet as reference (Φ = 55% in methanol).

Heptamethine dyes **2a,b** were prepared as FRET acceptors according to procedures developped by Peng[58] (Scheme S1) and were declined in hydrophobic (**2a**) and hydrophilic (**2b**) versions depending on the nature of the indolenium substituent (benzyl and propylsulfonate, respectively). They are designed in order to present optimized absorption at the Eu(III) emission wavelength (616 nm) and the presence of rigid *t*-Bu functionalized cyclohexenyl ring ensures good emission quantum yield in the NIR of 18% in dichloromethane that drops to 6% in water (Tab. 1, Fig. S1 and S2). $[Na]_3[Eu\mathbf{L}^{1G}_3]$ and **2a** was engaged as donor and acceptor respectively, in FRET experiment measured in dichloromethane solution. Upon increasing the amount of **2a**, a straightforward quenching of the Eu(III) emission was observed alongside with a decrease of the corresponding luminescence lifetime. (Tab. S1 and Fig. 2). The FRET efficiency η^{FRET} determined from the lifetime variations matches well the emission quenching and these results clearly show that **2a** is an excellent FRET acceptor for europium derivatives.

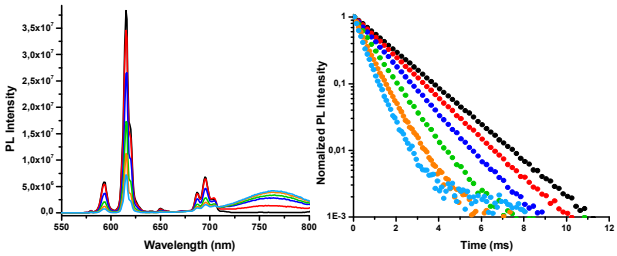

Fig. 2. Evolution of the Eu(III) and **2a** emissions (left) and lifetime (in log scale, right) of $[Na]_3[Eu\mathbf{L}^{1G}_3]$ upon addition of increasing amount of **2a** (black, 0 eq.; red, 0.3 eq.; blue 1.1 eq.; green 2.6, eq.; orange, 4.6 eq.; cyan, 7.7 eq.) in dichloromethane upon excitation at 360 nm.

Localization of $[Na]_3[EuL^{1G}_3]$ in fixed cells

$[Na]_3[Eu\mathbf{L}^{1G}_3]$ does not cross the plasma membrane of the living T24 cancer cells that were used in this work as a benchmark. The complex remains in the culture medium, is not cytotoxic up to 100 µM and is not internalized for up to 24 hours of incubation. That is why we first examined its intracellular localization in fixed cells. The 2P imaging was performed in slow scan mode to integrate maximum intensity in each pixel. $[Na]_3[Eu\mathbf{L}^{1G}_3]$ stains rapidly fixed permeabilized cells and accumulates differently in cellular sub-structures and organelles (Fig. 3). Most prominent localization is noted in the perinuclear cytoplasmic structures and the nucleoli, as it is the case of many cationic dyes.[59] We found that the labeling pattern can be partly altered by fixation, in particular comparing cold ethanol (Fig. 3A,B) and paraformaldehyde (PFA) procedures (Fig. 3C,D). In the case of ethanol fixation, the diffuse perinuclear accumulation of $[Na]_3[Eu\mathbf{L}^{1G}_3]$ is observed, which can be confused with a nuclear membrane or endoplasmic reticulum. This phenomenon disappeared in PFA fixed cells where homogeneous staining of the nucleosol is visible except the sites of nucleoli, while discrete organelles are distinguished in the cytoplasm. Mild PFA fixation is known to better preserve the native shape of biological structures keeping them hydrated. The higher resolution 3D deconvolution microscopy shows that these organelles in PFA-fixed cells have characteristic chaplet- and worm-like shapes similar to mitochondria (Fig. 3F).

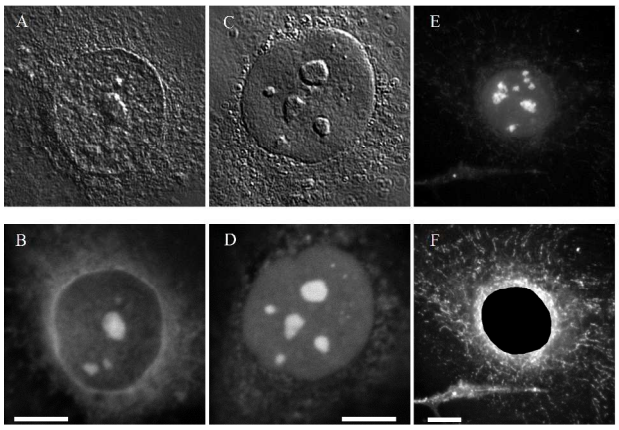

Fig. 3 Images of $[Na]_3[Eu\mathbf{L}^{1G}{}_3]$ loaded cells after cold EtOH (**A,B**) or paraformaldehyde (**C-F**) cell fixation. Images were taken in transmitted light DIC (**A,C**), two-photon laser scanning (**B,D**) and wide-field epifluorescence followed by 3D deconvolution (**E,F**). Panel **E** represents the same cell as **F** with the bright nuclear luminescence obstructed and the normalized intensity to reveal the less intense staining of the cytosol organelles. Scale bars 10 µm.

In order to get more insight in the localization pattern of $[Na]_3[Eu\mathbf{L}^{1G}{}_3]$, co-localization experiments in PFA-fixed cells were carried out with several organelle probes: MitoID, Acridine Orange, DiD, Golgin and DAPI, which are known to label mithochodria, nucleoli and lysosomes, membrane structures, Golgi apparatus and chromatin, respectively (Fig. S3, S4). These results confirm the preferential accumulation of the LLB in mitochondria, nucleoli and its diffuse localization in the nucleosol that does not correlate with the chromatin distribution.[13]

Live cell imaging

As already mentioned, live cultured T24 cells do not accumulate $[Na]_3[Eu\mathbf{L}^{1G}{}_3]$ if simply incubated in the presence of the dye. This feature is rather frequent for the lanthanide-organic complexes and efforts are on-going for the development of delivery framework for the intracellular imaging.[60]

However, it is possible to increase the cell membrane permeability by the physical or chemical treatments. In order to study the intracellular localization, interactions and to check for the possible cytotoxic effects of the probe, two different strategies were tested in this work: electroporation and mild permeabilization of the plasma membrane using saponin. The electroporation yielded unsatisfactory results, since the quantity of the probe entering the cell was not sufficient for the imaging and the rate of cell survival after treatment was too low. The second approach, however, was much more efficient and produced a strong accumulation of the complex in the punctuate structures in the cytoplasm of the treated cells (Fig. 4A, B, Movie S1). It should be stressed here that the saponin treatment in these conditions did not affect either viability of the cells or their capacity to proliferate once the solution was rinsed out.

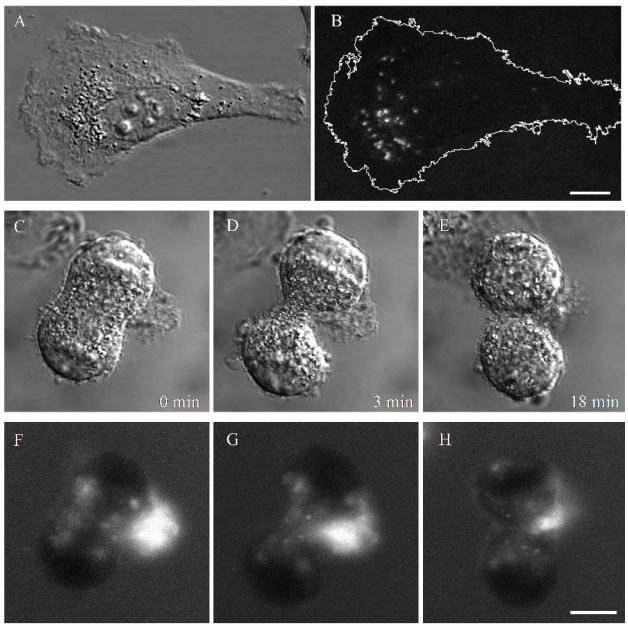

Fig. 4 Intracellular distribution of $[Na]_3[Eu\mathbf{L}^{1G}{}_3]$ in live cells after mild saponinpermeabilization. Spread living cell 1 h after the saponin and dye solution was rinsed out (**A, B**). Mitotic cell 24 h after treatment (**C-H**), dye solution was added to the culture medium after saponin rinsing out. Transmitted light DIC images of different stages of mitosis (**C-E**) and corresponding $[Na]_3[Eu\mathbf{L}^{1G}{}_3]$ 2P luminescence images (**F-H**). Scale bars 10 µm.

The distribution pattern and the intensity of the probe in cells did not change for at least 24 h of cell culturing regardless on the presence or absence of $[Na]_3[Eu\mathbf{L}^{1G}{}_3]$ in the culture medium. No nuclear localization was observed throughout the cell cycle. Even the disassembly of the nuclear envelope and the mixture of the nucleosol and cytosol content during mitosis did not result in a chromatin labeling (Fig. 4C). After mitosis, daughter cells inherited half of the total LLB charge (Fig. 4**C**-E) without any consequence on the following progression of cytokinesis and cell spreading. The absence of exocytosis and cytotoxicity combined with the inert behavior in cells make this compound a good candidate for a long-term cell tracking *in vivo*.

Time-gated imaging

The imaging of the long luminescence lifetime of europium complex was assessed here by two different implementations of the PSLIM method: 2P raster-scanning and 1P line-scanning. Pinhole shifting approach, based on the pioneering work of Ramshesh and Lemasters,[53] takes advantage of the spatial spread of a long luminescence signal in scan direction. This spread is dependent on the ratio of the luminescence lifetime and the pixel dwell time, as illustrated in Fig. 5 that was imaged with the open confocal pinhole (scanning from left to right). As the scanning speed increases, streaks appear on the right edge of the cell image whereas the left edges stay well defined (Fig. 5B, C). These persisting light streaks are due to the fact that luminescent lifetime of the europium species is much longer than the pixel dwell time. This apparent drawback, which can be partially alleviated by reducing the pinhole diameter, turns out to be a real advantage for TG-imaging.

Indeed, it allows the selective sampling of the delayed, TG luminescence signal, by closing the pinhole to 1 AU and lagging

it by one or more AUs (Fig. 5D). The emission of the short living species or tissue autofluorescence can thus be specifically attenuated, while the decrease of the long-living Eu(III) luminescence is much less significant. For instance, in our conditions the pinhole lagging of 1 AU resulted in 3-fold attenuation in the channel of short living DNA probe Hoechst while almost no decrease occurred in Eu(III) channel (Fig. 5F,G). One can also notice a slightly lower contrast of Eu(III) image after the pinhole shift resulting from pixel cross-talk. The imaging speed in the raster scanning mode is limited by the necessarily long pixel dwell time and is here more than 20 s/image (177 µs/pixel).

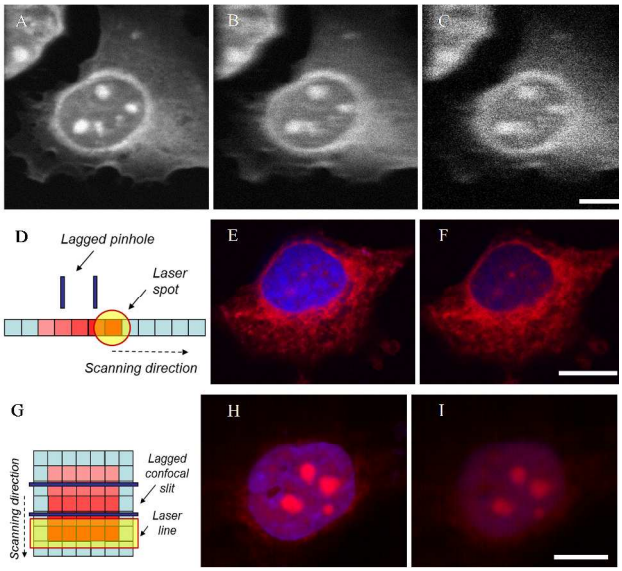

Fig. 5 Light streaks of $[Na]_3[EuL^{IG}_3]$ luminescence appear at higher scanning speed (**A**, 204.8 µs/pixel; **B**, 25.6 µs/pixel; **C**, 2.5 µs/pixel) (λ_{exc}= 740 nm, pinhole open). Raster scanning was performed horizontally, from left to right. Schematic presentation of the principle of pinhole shifting in raster- (**D**) and line-scanning (**G**) microscopy. The lagged positions of the pinhole or the confocal slit are presented by dark blue lines, the long lifetime luminescence emission is in red scales. (**E**, **F**, **H**, **I**) images of the fixed cells stained with $[Na]_3[EuL^{IG}_3]$ (red) and Hoechst (blue). Images were acquired with the 1AU-pinhole aligned to the laser spot (**E**) or lagged by 1AU (**F**), and with the confocal slit aligned to the laser line (**H**) or lagged by 1AU (**I**). Relative channel intensities reflect a 3-fold attenuation of the short-lifetime blue fluorophore comparing to Eu LLB. Scale bars 10 µm.

We extended the PSLIM approach to a much faster line scanning imaging using LSM7 LIVE confocal microscope with 1P excitation at 405 nm of the same couple of probes. The principle of the line scanning consists in profiling the excitation laser beam into a narrow line (Fig 5G**)** and detecting the whole row of pixels with the line-CCD detector. The confocality in this case is assured by a thin slit positioned in the detection light path. In order to selectively detect the delayed luminescence signal, the confocal slit was closed to 1 AU and shifted by 1 AU in lagging direction. This resulted in > 2.5 fold specific attenuation of Hoechst, similar to that obtained in the raster scanning mode (Fig 5I, J). The overall acquisition time of the image was much shorter (< 1 s/image), while keeping a pixel dwell time long enough for the luminescence integration. The scanning speed of LSM7 LIVE can be further increased making line PSLIM well suited for the rapid selective imaging of long-lifetime probes in living cells as well as 3D applications. The probes with less brightness can in principle be suited for the line-scanning imaging, due to longer pixel dwell time. Nevertheless our test experiments witnessed lower sensitivity of the line CCD detector of LSM7 LIVE as compared to the PMT of LSM710, which was only partially compensated by the longer integration time.

Actually LSM7 LIVE line-scanning confocal module is only available with 1P excitation but there are no fundamental limitations for 2P excitation in line or parallel multispot configuration (e.g. TriM-Scope, LaVision). Introducing lagged confocal slit or a pinhole array in this case would allow 2P-PSLIM, which could be particularly useful for *in vivo* imaging of 2P-LLBs.

Luminescence decay measurement

We show in the present work that the long (µs to ms) luminescence lifetimes can be measured with high accuracy and mapped using the standard *commercial* confocal microscope. This temporal decay sampling is realized in a pixel-by-pixel or line-by-line mode using the fluorescence recovery after photobleaching (FRAP) configuration with the deactivated sampling laser. In this case, performing FRAP in a single spot mode, a short pulse of light is shaped by AOTF from the "bleaching" laser and sent to the specimen. The emitted luminescence is then sampled by the confocal detector at high rate (> 1 MHz) without further excitation. The sampling continues until the decay reaches the noise level, thus setting almost no upper limit for the measured lifetimes. The lower limit is set by the microscope electronics (the shortest pixel dwell time of LSM710 is 0.64 µs).

The proof-of-principle experiments were carried out using $[Na]_3[EuL^{IG}_3]$ microcrystals with a 405 nm one-photon or a 740 nm 2P excitation (Fig. 6A). The decay was sampled by the 12-bit photomultiplier in a narrow spectral band around the main emission peak at 615 nm, characteristics of europium. Low intensity excitation pulses were used to avoid photobleaching and thermal effects. The emission intensity presented the exponential profile but the signal-to-noise ratio of the single measurement was rather bad (Fig. 6B). The acquisition was thus repeated 100 times in the same spot (total acquisition time ~1 s) and the average decay was successfully fitted by the monoexponential decay model (Fig. 6C). The lifetime in different positions of the microcrystal was highly reproducible with the average value of 1.14 ± 0.05 ms. Identical values were obtained with 405 nm excitation and at different laser power.

For comparison, the luminescence lifetime in the solid state was also determined independently using a conventional fluorimeter with a 1P excitation (xenon lamp) yielding a value of 1.2 ms.

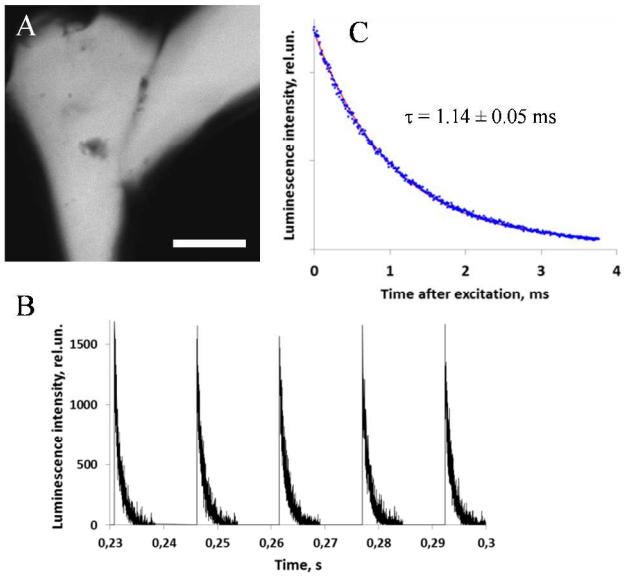

Fig. 6 A) Two-photon image of $[Na]_3[Eu\mathbf{L}^{1G}{}_3]$ microcrystals. Scale bars 10 µm. B) Example decays in a series of acquisition in a single spot. C) Average of 100 decays (blue dots) is successfully fitted with a monoexponential model (red solid line).

It should be noted that rapid decay sampling implies a very short and well defined detector integration time. Any uncertainty of this value affects the measured decay time. In our experience, differences between the tested confocal systems LSM510 and LSM710 were about 10% when using the shortest integration time (data not shown) probably because of the electronic dead time during the signal read-out. This difference between microscopes can be reduced using longer integration time, but, in general, the *absolute* lifetime values measured with a given commercial system need to be calibrated. It should be stressed however, that the values obtained with the *same* system at the *same* sampling rate are highly reproducible and allow precise comparison of luminescence decays within the sample.

Lifetime and resonance energy transfer imaging

The luminescence lifetime imaging of the $[Na]_3[Eu\mathbf{L}^{1G}{}_3]$ loaded cells was performed by the spot-by-spot mapping of the region of interest using TSLIM, implemented as a macro in Zen2010 software of the LSM710 microscope. A series of 100 decays in each spot was measured (acquisition time ~1 s) and registered in a single file and the scanner was positioned in the neighboring spot with a step of 1 µm. An image of 20x21 points in a fixed cell was acquired in approximately 25 min. The data treatment was automated using a home written MatLab procedure, based on the Gauss-Newton non-linear fitting with the bi-exponential model. The weighted averaged decay in each spot was calculated, color coded and plotted without decay intensity weighting (Fig.S5). The luminescence lifetime of $[Na]_3[Eu\mathbf{L}^{1G}{}_3]$ alone was found to be remarkably homogeneous throughout the cell. No correlation between lifetime and intensity was observed. The mean lifetime in PFA fixed cells (1.02±0.06 ms) was almost similar that in EtOH fixed cells (1.07±0.06 ms). Interestingly this result shows that no dissociation of the complex, observed by a strong decrease of the lifetime,[13] occurs upon internalization in the cell, confirming its potential for the bio-imaging applications. The precision of TSLIM allows reliable tracing of lifetime variations as small as 0.1% in cells, thus making it a very sensitive tool for mapping the physical-chemical factors or ion sensing…[29] using the LLBs.

In order to demonstrate the potential of the long lifetime imaging, an intracellular FRET experiment was undertaken involving $[Na]_3[Eu\mathbf{L}^{1G}{}_3]$ and the hydrosolublepolymethine derivative **2b** acting as FRET acceptor. It is anticipated that FRET will occur depending on co-localization of the $[Na]_3[Eu\mathbf{L}^{1G}{}_3]$ complex and **2b** in the cell resulting in a decrease of the Eu(III) lifetime and that the magnitude of this decrease will depend on the relative local concentration of the two partners (vide infra). Preliminary cell labeling experiment with **2b** alone indicates an intracellular localization rather similarwith $[Na]_3[Eu\mathbf{L}^{1G}{}_3]$, albeit with the different ratio of mitochondrial to nucleolar accumulation (Fig. S6). The fixed cells were then co-stained with $[Na]_3[Eu\mathbf{L}^{1G}{}_3]$ and **2b**.The values of the Eu(III) luminescence lifetime, measured by TSLIM in the presence of FRET acceptor were considerably lower and much more heterogeneous throughout the cell than those of $[Na]_3[Eu\mathbf{L}^{1G}{}_3]$ alone (Fig. 7C). The corresponding FRET efficiency (calculated from lifetime variationsTable S1) varied between 30% and 40%, with the highest values found in a perinuclear region, while the lowest values were revealed in nucleoli. This result correlates well with the different relative accumulation of donor and acceptor species in these subcellular structures (Fig.7D, E). In case of nonspecific intermolecular associations the percentage of interacting donor molecules depends on the availability of the acceptor within the Förster distance. Thus acceptor to donor ratio modulates the apparent FRET efficiency in different pixels; the higher ratio correlates to the higher FRET (Fig. 7Fand spectroscopy experiments Fig. 2).

It should be underlined, that this result could be completely different if obtained by the conventional TG-imaging techniques, since apparent FRET intensity map would reflect both donor local concentration and the luminescence quenching by the acceptor. TSLIM, on the contrary, takes into account the donor lifetime regardless its concentration, thus mapping more accurate FRET efficiency.

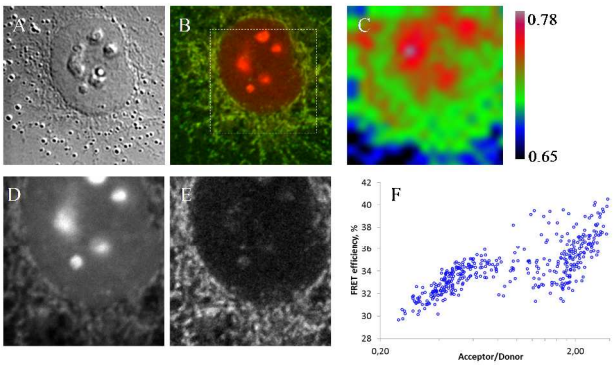

Fig. 7 FRET imaging by TSLIM of the PFA-fixed cell loaded with $[Na]_3[Eu\mathbf{L}^{1G}{}_3]$ (donor) and **2b** (acceptor). **A** - Transmitted light DIC image of the cell. **B** – Overlay of the europium luminescence (red) and **2b** fluorescence (green). Dashed rectangle limits the region measured by TSLIM. **C** – Distribution of $[Na]_3[Eu\mathbf{L}^{1G}{}_3]$ lifetime values, **D** and **E** – distribution of donor and acceptor intensities. **F** - Scatter plot of FRET efficiency versus acceptor to donor intensity ratio. Each blue circle represents one pixel of the 20x21 map.

The major inconvenience of the TSLIM imaging in the spot-by-spot mode is a long acquisition time, resulting from the measurement itself, but also largely from delays of the software/hardware communications in confocal microscope, multiplied by the number of spots in the image. In the previous example, 25 min total time (for the 421 spots) included only 7 min of signal acquisition. To overcome this drawback, the parallel detection line scanning confocal microscope as LSM7 LIVE can be potentially used for much faster TSLIM measurements. The line sampling allows 1 - 2 orders of magnitude faster lifetime imaging. Its principle is similar to the TSLIM in spot mode and takes advantage of the standard FRAP configuration in a 'line' mode with the deactivated sampling laser. In this case, a whole row of up to 512 pixels is simultaneously excited by a short pulse of the 'bleaching' laser, and the luminescence decay is then temporally sampled in all pixels of the line simultaneously by a line-CCD detector. The proof-of-principle experiment is presented in Fig. S7. The 128x60 pixel lifetime image with 50 µs sampling time was acquired in less than 2 min, while the signal to noise ratio was improved by the averaging of 10 repetitions of each line. The effective temporal resolution achieved in this experiment was only 128 µs because of the long detector readout and electronic dead-time but it was sufficient to sample the millisecond luminescence decay. This example illustrates a great potential of parallel sampling of long lifetime of LLBs that can be further improved using more sensitive detector arrays, such as line EM-CCD or GaAsPPMTs.

Conclusion

In this article we demonstrated that a commercial confocal microscope without any modifications or additional equipments can perform time-gated imaging (PSLIM) or long lifetime imaging (TSLIM) in µs to ms range under classical 1P or nonlinear 2P excitations. In addition, PSLIM and TSLIM techniques were extended to the more rapid line-scanning mode. The extraordinary potentialities of PSLIM and TSLIM techniques have been illustrated using $[Na]_3[Eu\mathbf{L^{1G}}_3]$, a well knownEuropium based 2P-LLB. Its localization in fixed and living cells was characterized by 2P microscopy and precise measurement of its long luminescence lifetime was conducted *in cellulo* using a commercial microscope in TSLIM mode. Using $[Na]_3[Eu\mathbf{L^{1G}}_3]$ as donor in conjunction with an organic heptamethine dyes, TSLIM allows quantifying 2P-FRET in different cellular compartments independently on probe concentration. On the other hand, pinhole shifting confocal imaging (PSLIM) in classical or in faster line scanning mode allowed selective Eu(III) visualization in the presence of short lifetime DNA label Hoechst. Taken together TSLIM and PSLIM techniques allow to fully exploit the spectral but also the temporal peculiar properties of lanthanide luminescent bioprobes under 1 or 2P excitation and open new avenues for the detailed study of lanthanide biosensors or FRET detection*in cellulo* or *in-vivo.*

Experimental Section

Synthesis

NMR spectra (^1H, ^{13}C) were recorded at room temperature on a BRUKER® Avance operating at 500.10 MHZ and 125.75 MHz for ^1H and ^{13}C, respectively. ^{13}C NMR spectra were recorded using the µDEFT experiment[61] and signals were assigned using HSQC and HMBC experiments. Data are listed in parts per million (ppm) and are reported relative to residual solvent peaks being used as internal standard (^1H ($CDCl_3$): 7.26 ppm, ^{13}C ($CDCl_3$): 77.2 ppm; ^1H (CD_3OD): 3.31 ppm, ^{13}C (CD_3OD): 49.0 ppm; ^1H (DMSO-d6): 2.50 ppm, ^{13}C (DMSO-d6): 39.5 ppm). High resolution mass spectrometry measurements were performed at Centre Commun de Spectrometrie de Masse (Villeurbanne, France). Starting materials were purchased from Sigma Aldrich®, Acros Organics® or Alfa Aesar® with the best available quality grade. All reactions were routinely performed under argon atmosphere in anhydrous solvents. Column chromatography was performed using Acros Organics® (0.035-0.070 mm) silicagel. All reagents were purchased from commercial sources and used without further purification, otherwise noted. Compounds **1a** and $[Na]_3[Eu\mathbf{L^{1G}}_3]$ were prepared according to published procedures.[13, 62]

Compound 2a. A solution of 440 mg of **1a** (0.57 mmol, 1 eq.) and 0.19 mL of distilled propylamine (2.28 mmol, 4 eq.) in 5 mL of anhydrous dimethylformamide (DMF) was stirred for 45 minutes at 70°C. The reaction mixture was allowed to cool to RT, added by 20 mL of dichloromethane (DCM) and washed three times with an aqueous solution of HBr (1M). The organic layer was dried over Na_2SO_4 and finally concentrated. The crude residue was purified by flash chromatography on silica DCM/EtOAc/MeOH (from 50/50/0 to 45/45/10) to afford **2a** as a glossy blue solid in a 93% yield (420 mg). ^1H NMR ($CDCl_3$, 500.10 MHz): δ 9.95 (s, 1H), 7.62 (d, $^3J_{trans}$ = 13 Hz, 2H), 7.33-7.26 (m, 8H), 7.24-7.18 (m, 6H), 7.04 (t, ^3J = 7 Hz, 2H), 6.83 (d, ^3J = 8 Hz, 2H), 5.45 (d, $^3J_{trans}$ = 12 Hz, 2H), 4.97 (d, ^2J = 16 Hz, 2H), 4.89 (d, ^2J = 17 Hz, 2H), 3.77 (m, 2H), 2.31 (d, ^2J = 13 Hz, 2H), 2.02 (m, 2H), 1.76 (s, 6H), 1.71 (s, 6H), 1.65 (m, 2H), 1.20 (m, 1H), 0.91 (t, ^3J = 6 Hz, 3H), 0.76 (s, 9H). ^{13}C NMR ($CDCl_3$, 125.75 MHz): δ 171.0, 166.0, 143.9, 140.2, 137.2, 135.4, 129.2, 128.2, 127.9, 126.5, 122.4, 122.3, 121.4, 107.8, 94.8, 51.5, 47.5, 47.0, 43.7, 32.6, 29.2, 29.1, 27.1, 26.7, 24.2, 11.4. UV-Vis (CH_3OH) λ_{max} = 617 nm (ε_{max} = 95,800 $L.mol^{-1}.cm^{-1}$). UV-Vis (DCM) λ_{max} = 652 nm (ε_{max} = 102,000 $L.mol^{-1}.cm^{-1}$). MS (ESI+): $[M]^+$ = 714.4797 (calcd for $C_{51}H_{60}N_3$: 714.4782).

Compound 2b. A solution of 90 mg of **1b** (0.12 mmol, 1 eq.) and 0.04 mL of distilled propylamine (0.48 mmol, 4 eq.) in 3 mL of anhydrous DMF was stirred for 2h at 50°C. The reaction mixture was allowed to cool to RT and concentrated under reduced pressure. The crude residue was purified by flash chromatography on silica using acetonitrile/water (95:5 to 90:10) as eluent to afford the product **2b** as a glossy blue solid in a 45 % yield (42 mg). ^1H NMR ($CDCl_3$, 500.10 MHz): δ 7.76 (d, $^3J_{trans}$ = 12 Hz, 2H), 7.36 (d, ^3J = 7 Hz, 2H), 7.30 (t, ^3J = 7 Hz, 2H), 7.15 (d, ^3J = 8 Hz, 2H), 7.08 (t, ^3J = 7 Hz, 2H), 4.16 (m, 4H), 3.74 (t, ^3J = 6 Hz, 2H), 2.94 (t, ^3J = 7 Hz, 4H), 2.82 (d, ^2J = 11 Hz, 2H), 2.23 (t, ^3J = 7 Hz, 4H), 2.06 (m, 2H), 1.83 (m, 2H), 1.67 (s, 6H), 1.66 (s, 6H), 1.41 (m, 1H), 1.07 (s, 9H), 1.04 (t, ^3J = 7 Hz, 3H). ^{13}C NMR ($CDCl_3$, 125.75 MHz): δ 171.6, 168.9, 144.4, 141.2, 140.5, 129.5, 123.8, 123.0, 122.7, 110.1, 95.7, 58.3, 53.4, 48.5, 46.2, 42.8, 33.7, 29.2, 29.1, 27.8, 27.8, 25.8, 23.5, 11.7. UV-Vis (CH_3OH) λ_{max} = 605 nm (ε_{max} = 49,000 $L.mol^{-1}.cm^{-1}$). UV-Vis (CH_2Cl_2) λ_{max} = 623 nm (ε_{max} = 68,000 $L.mol^{-1}.cm^{-1}$). MS (ESI+):

$[M+2Na]^+$ = 822.3545 (calcd for $C_{43}H_{58}N_3Na_2O_6S_2^+$: 822.3557).

Photophysical measurements in solution

Absorption spectra were recorded on a JASCO V-650 spectrophotometer in spectrophotometric grade methanol, water or dichloromethane solutions (ca. 10^{-5} or 10^{-6}mol L^{-1}). Molar extinction coefficients (ε) were determined at least two times. Emission spectra were measured using a Horiba-Jobin-Yvon Fluorolog-3 iHR320 fluorimeter. The steady-state luminescence was excited by unpolarized light from a 450 W xenon CW lamp and detected at an angle of 90° for diluted solution measurements (10 mm quartz cuvette) by Hamamatsu R928 photomultiplier tube. Spectra were corrected for both the excitation source light intensity variation and the emission spectral response. Phosphorescence lifetimes (> 30 µs) were obtained by pulsed excitation using a FL-1040 UP Xenon Lamp. Luminescence decay curves were fitted by least-squares analysis using Origin®. Short luminescence decay was monitored using the TC-SPC Horiba apparatus using Ludox in distilled water to determine the instrumental response function used for deconvolution. Excitation was performed using Nanoled-570 (peak wavelength 573 nm, duration 1.5 ns) and the deconvolution was performed using the DAS6 fluorescence-decay analysis software. Luminescence quantum yields Q were measured in diluted water solution with an absorbance lower than 0.1 using the following equation $Q_x/Q_r = [A_r(\lambda)/A_x(\lambda)][n_x^2/n_r^2][D_x/D_r]$ were A is the absorbance at the excitation wavelength (λ), n the refractive index and D the integrated luminescence intensity. "r" and "x" stand for reference and sample. Here, reference is quinine bisulfate in 1N aqueous sulfuric acid solution (Q_r = 0.546) or cresyl violet in methanol (Q_r = 0.55). Excitation of reference and sample compounds was performed at the same wavelength.

Cell culturing and treatment

We used T24 human epithelial bladder cancer cell line (ATCC No HBT-4). In our experiments, T24 cells were cultured in 25 cm^2 tissue-culture flasks (T25) at 37°C, in a humidified atmosphere with 5% CO_2. They were incubated in RPMI 1640 supplemented with 100 U/mL penicillin, 100 µg/mL streptomycin, and 10% fetal calf serum (complete medium). Cells were grown to near confluence in the culture flasks and then suspended with 0.05% trypsin–EDTA solution (Sigma).

Twenty-four hours before experiments, cells were placed on LabTek I chambered cover glass (Nunc) at low cell density in complete culture medium. After being washed with the phosphate buffer saline (PBS), cells were fixed using paraformaldehyde (PFA3% in PBS) for 10 min, permeabilized with PBS containing 0.5% Triton X100 for 10 min, and then washed with PBS. For gentle permeabilization of living cells, they were incubated 45 min at 37°C in the presence of 15 µg/ml saponin and $5x10^{-4}$ M $[Na]_3[Eu\mathbf{L}^{\mathbf{1G}}_3]$ in complete medium, washed twice with PBS, before addition of complete medium. For electroporation experiments, cells were trypsinized, and pelleted by centrifugation. The cell pellets were resuspended in 1 ml appropriate medium with 5.10^{-4} M $[Na]_3[Eu\mathbf{L}^{\mathbf{1G}}_3]$, transfected using an Amaxa Cell Line Nucleofector Kit R (Lonza) and electroporated using an Amaxaelectroporator (Lonza).

Microscopy

All confocal experiments were performed using a LSM-DuoScan NLO microscope (Carl Zeiss) composed of LSM710 *raster* scanning and LSM7 LIVE *line* scanning confocal modules attached to the inverted motorized stand (AxioObserver) equipped with the on-stage cell incubator. The excitation was provided by either 405nm DPSS cw laser (for line- and raster scanning) or Ti:Sa femtosecond tunable laser (Chameleon, Ultra II, Coherent) for 2P excitation in raster scanning mode. Zen2010 acquisition software controlled both the two scanning units, the pinhole alignment, the AOTF pulse shaping and the motorized sample stage. The plan-apochromat 63x/1.4 oil immersion objective was used throughout experiments. The pinhole (LSM710) and the confocal slit (LSM7 LIVE) were set to 1 AU for confocal 1P microscopy, while the LSM710 pinhole was open during 2P acquisition. The size of the Airy diffraction disk (AU) is determined by the lateral resolution of the confocal microscope r_{xy}=0.4λ/NA, where λ is the wavelength of light and NA is the numerical aperture of the objective lens.

The wide-field 3D imaging of $[Na]_3[Eu\mathbf{L}^{\mathbf{1G}}_3]$ loaded cells was performed with an Axiovert 200M inverted microscope (Carl Zeiss), plan-apochromat 63x/1.4 objective and X-Cite HBO excitation in epifluorescence mode. The long-pass DAPI filter set (49) was modified by replacing the emission filter by BP 629/62 HE (AHF Analysentechnik, Germany) to assure the Eu excitation in near-UV and the selective detection of its red emission. 3D-stacks were acquired in stream mode with CoolSNAP HQ^2 CCD camera (Roper scientific) and ASI 2000 piezo stage with 0.2 µm axial step and deconvoluted with the measured point spread function using the Meinel iterative algorithm of MetaMorph software (Universal Imaging). The number of iterations was limited to 8 in order to avoid possible noise artifacts.

Temporal sampling lifetime imaging microscopy (TSLIM)

We used commercial laser scanning microscopes for precise luminescence lifetime measurements in the µs-ms range using the integrated AOTF and PMT or line-CCD detectors. We validated the TSLIM approach using both the *raster* scanning LSM 710 and the rapid *line* scanning LSM7 LIVE confocal units (Carl Zeiss), the former was also used with 2P excitation and descanned detection.

The time series acquisition for TSLIM was configured in a single spot (LSM710) or a single line (LSM7 LIVE) using the standard FRAP module of Zen2010 software. Sampling laser was deactivated, while the 'bleaching' laser was allowed to produce a single low intensity pulse (few µs) for the excitation light source. Decay sampling started immediately after the excitation pulse with 7.56 µs (LSM710) or 50 µs (LSM7 LIVE) temporal resolution. The whole procedure was repeated 100 times (total time per spot/line ~1 s) and the average decay was registered as a separate file. The macro interface of Zen2010 was used to move the sample stage to the next position and to loop the acquisition. The luminescence lifetime of $[Na]_3[Eu\mathbf{L}^{\mathbf{1G}}_3]$ in fixed cells was measured in the selected regions of interest (zoom 4) divided into 20x21 equidistant (1 µm) sampling spots (LSM710) or 60 lines of 128 pixels (optical zoom 1) spaced by 1 µm (LSM7 LIVE).

The lifetime analysis was performed by the nonlinear fitting with single- or bi-exponential models. The mean luminescence decay was obtained by averaging all individual decays acquired in each spot. Thus, the experimental data are constituted by *n*pairs

(t_k, Z^k_{exp}), $k = 1, 2, \ldots n$, where $Z^k_{exp} = (Z^k_{ij})$ is the matrix of luminescence intensity corresponding to the t_k time and (ij) location in the image.

The relationship between time t and the luminescence at location (ij) is modeled as a biexponential decay using two time scales ($\tau_{1,ij}$ and $\tau_{2,ij}$) and reads

$$Z_{th}(t; \theta_{ij}) = \alpha_{1,ij}\exp(-t/\tau_{1,ij}) + \alpha_{2,ij}\exp(-t/\tau_{2,ij}) + \beta_{ij}$$

where $\alpha_{1,ij}$ and $\alpha_{2,ij}$ are relative contributions of two components, β_{ij} is the asymptotic luminescence intensity and $\theta_{ij} = (\alpha_{1,ij}, \alpha_{2,ij}, \tau_{1,ij}, \tau_{2,ij}, \beta_{ij})$ is a global notation for the whole set of parameters. For each location (ij) the optimal values of these five parameters are determined by minimizing the following objective function

$$\chi^2(\theta_{ij}) = \Sigma_k(Z_{th}(t; \theta_{ij}) - Z^k_{exp,ij})^2$$

which expresses the distance between the experimental data and the theoretical model in the sense of the least squares. This minimization problem is solved by a numerical procedure based on the Gauss-Newton method using exact evaluation of the jacobian matrices. The used algorithm needs an initial estimation of the parameter values for each optimal set to determine. In order to automatically compute the optimal values of parameter sets corresponding to each location in image, only the initial guess corresponding to the first location is manually determined (mainly by graphical investigation). Next, the initial guess related to the location $\ell + 1$ is chosen as the optimal set related to the location ℓ. To avoid spurious optimal set of values, the initial estimation (location = 00) must be chosen so that $\alpha_{1,00} \neq \alpha_{2,00}$ and $\tau_{1,00} \neq \tau_{2,00}$.

The average lifetime values in each spot were then color coded and plotted as lifetime images with no intensity weighting. The corresponding intensity image was obtained via decay integration in each pixel. The curve fitting algorithm is written as a Matlab routine and a simplified version for the monoexponential analysis as an ImageJ macro. The FRET efficiency E_{FRET} in each pixel (ij) was calculated as follows:

$$E_{FRET,ij} = (1 - \tau_{d,ij}/\tau_0)\cdot 100\%$$

where, $\tau_{d,ij}$ – is the measured average luminescence lifetime of the donor and τ_0 – is the reference donor lifetime in the absence of acceptor.

Acknowledgement

The authors thank ARC, Ligue Nationale contre le cancer (Comité de la Drôme) and CPER program for the financial support of the confocal microscopy facilities.

Notes and references

[a] *INSERM, IAB, F-38000, Grenoble, France*
[b] *Univ. Grenoble Alpes, IAB, F-38000, Grenoble, France*
[c] *CHU de Grenoble, IAB, F-38000, Grenoble, France*
[d] *University Lyon 1, ENS Lyon, CNRS UMR 5182, 46 allée d'Italie 69364 Lyon, France. olivier.maury@ens-lyon.fr*
[e] *Univ. Grenoble Alpes, LIPHY, F-38000, Grenoble, France*
CNRS, LIPHY, F-38000, Grenoble, France

† Electronic Supplementary Information (ESI) available: synthesis Scheme, complete spectroscopic characterizations of **2a**, **2b** and related synthetic intermediates, additional microscopy imaging experiments and a movie of stained living cells. See DOI: 10.1039/b000000x/

1. S. V. Eliseeva and J.-C. G. Bunzli, *Chem. Soc. Rev.*, 2010, **39**, 189-227.
2. J.-C. Bünzli and S. Eliseeva, in *Lanthanide Luminescence*, eds. P. Hänninen and H. Härmä, Springer Berlin Heidelberg, 2011, vol. 7, ch. 3, pp. 1-45.
3. C. P. Montgomery, B. S. Murray, E. J. New, R. Pal and D. Parker, *Acc. Chem. Res.*, 2009, **42**, 925-937.
4. E. G. Moore, A. P. S. Samuel and K. N. Raymond, *Acc. Chem. Res.*, 2009, **42**, 542-552.
5. J.-C. G. Bünzli, *Chem. Rev.*, 2010, **110**, 2729-2755.
6. C. Andraud and O. Maury, *Eur. J. Inorg. Chem.*, 2009, **2009**, 4357-4371.
7. Y. Ma and Y. Wang, *Coord. Chem. Rev.*, 2010, **254**, 972-990.
8. G. Piszczek, B. Maliwal, I. Gryczynski, J. Dattelbaum and J. Lakowicz, *J. Fluoresc.*, 2001, **11**, 101-107.
9. M. H. V. Werts, N. Nerambourg, D. Pelegry, Y. L. Grand and M. Blanchard-Desce, *Photochem. Photobiol. Sci.*, 2005, **4**, 531-538.
10. L.-M. Fu, X.-F. Wen, X.-C. Ai, Y. Sun, Y.-S. Wu, J.-P. Zhang and Y. Wang, *Angew. Chem., Int. Ed.*, 2005, **44**, 747-750.
11. A. D'Aléo, A. Picot, P. L. Baldeck, C. Andraud and O. Maury, *Inorg. Chem.*, 2008, **47**, 10269-10279.
12. G. S. He, L.-S. Tan, Q. Zheng and P. N. Prasad, *Chem. Rev.*, 2008, **108**, 1245-1330.
13. A. Picot, A. D'Aléo, P. L. Baldeck, A. Grichine, A. Duperray, C. Andraud and O. Maury, *J. Am. Chem. Soc.*, 2008, **130**, 1532-1533.
14. G.-L. Law, K.-L. Wong, C. W.-Y. Man, W.-T. Wong, S.-W. Tsao, M. H.-W. Lam and P. K.-S. Lam, *J. Am. Chem. Soc.*, 2008, **130**, 3714-3715.
15. F. Kielar, A. Congreve, G.-l. Law, E. J. New, D. Parker, K.-L. Wong, P. Castreno and J. de Mendoza, *Chem. Commun.*, 2008, 2435-2437.
16. S. V. Eliseeva, G. Auböck, F. van Mourik, A. Cannizzo, B. Song, E. Deiters, A.-S. Chauvin, M. Chergui and J.-C. G. Bünzli, *J. Phys. Chem. B*, 2010, **114**, 2932-2937.
17. Z.-J. Hu, X.-H. Tian, X.-H. Zhao, P. Wang, Q. Zhang, P.-P. Sun, J.-Y. Wu, J.-X. Yang and Y.-P. Tian, *Chem. Commun.*, 2011, **47**, 12467-12469.
18. W.-S. Lo, W.-M. Kwok, G.-L. Law, C.-T. Yeung, C. T.-L. Chan, H.-L. Yeung, H.-K. Kong, C.-H. Chen, M. B. Murphy, K.-L. Wong and W.-T. Wong, *Inorg. Chem.*, 2011, **50**, 5309-5311.
19. T. Zhang, X. Zhu, C. C. W. Cheng, W.-M. Kwok, H.-L. Tam, J. Hao, D. W. J. Kwong, W.-K. Wong and K.-L. Wong, *J. Am. Chem. Soc.*, 2011, **133**, 20120-20122.
20. T. Zhang, X. Zhu, W.-K. Wong, H.-L. Tam and W.-Y. Wong, *Chem. Eur. J.*, 2013, **19**, 739-748.
21. A. D'Aléo, A. Bourdolle, S. Brustlein, T. Fauquier, A. Grichine, A. Duperray, P. L. Baldeck, C. Andraud, S. Brasselet and O. Maury, *Angew. Chem., Int. Ed.*, 2012, **51**, 6622-6625.
22. G. Marriott, R. M. Clegg, D. J. Arndt-Jovin and T. M. Jovin, *Biophys. J.*, 1991, **60**, 1374-1387.
23. J. Yuan and G. Wang, *J. Fluoresc.*, 2005, **15**, 559-568.
24. G. Vereb, E. Jares-Erijman, P. R. Selvin and T. M. Jovin, *Biophys. J.*, 1998, **74**, 2210-2222.
25. S. Phimphivong and S. S. Saavedra, *Bioconjugate Chem.*, 1998, **9**, 350-357.
26. A. Beeby, S. W. Botchway, I. M. Clarkson, S. Faulkner, A. W. Parker, D. Parker and J. A. G. Williams, *J. Photochem. Photobiol., B*, 2000, **57**, 83-89.
27. D. Parker, *Coord. Chem. Rev.*, 2000, **205**, 109-130.

28. R. Carr, N. H. Evans and D. Parker, *Chem. Soc. Rev.*, 2012, **41**, 7673-7686.
29. S. Pandya, J. Yu and D. Parker, *Dalton Trans.*, 2006, 2757-2766.
30. S. Mizukami, K. Tonai, M. Kaneko and K. Kikuchi, *J. Am. Chem. Soc.*, 2008, **130**, 14376-14377.
31. S. J. Butler, B. K. McMahon, R. Pal, D. Parker and J. W. Walton, *Chem. Eur. J.*, 2013, **19**, 9511-9517.
32. M. Rajendran, E. Yapici and L. W. Miller, *Inorg. Chem.*, 2013, **53**, 1839-1853.
33. A. K. Hagan and T. Zuchner, *Anal. Bioanal. Chem.*, 2011, **400**, 2847-2864.
34. J. M. Zwier, H. Bazin, L. Lamarque and G. Mathis, *Inorg. Chem.*, 2014, **53**, 1854-1866.
35. I. Hemmilä and S. Webb, *Drug Discov. Today*, 1997, **2**, 373-381.
36. F. Degorce, A. Card, S. Soh, E. Trinquet, G. P. Knapik and B. Xie, *Curr. Chem. Genomics*, 2009, **3**, 22-32.
37. P. Ollikka, A. Ylikoski, A. Kaatrasalo, H. Harvala, H. Hakala and J. Hovinen, *Bioconjugate Chem.*, 2008, **19**, 1269-1273.
38. J. Vuojola, U. Lamminmäki and T. Soukka, *Anal. Chem.*, 2009, **81**, 5033-5038.
39. K. Hanaoka, K. Kikuchi, S. Kobayashi and T. Nagano, *J. Am. Chem. Soc.*, 2007, **129**, 13502-13509.
40. K. Hanaoka, *Chem. Pharm. Bull.*, 2010, **58**, 1283-1294.
41. N. Gahlaut and L. W. Miller, *Cytometry Part A*, 2010, **77A**, 1113-1125.
42. D. Geißler, S. Linden, K. Liermann, K. D. Wegner, L. J. Charbonnière and N. Hildebrandt, *Inorg. Chem.*, 2013, **53**, 1824-1838.
43. D. Jin, J. Piper, J. Yuan and R. Leif, Time-gated real-time bioimaging system using multicolor microsecond-lifetime silica nanoparticles, Proc. SPIE 7568, 2010.
44. Y. Lu, P. Xi, J. A. Piper, Y. Huo and D. Jin, *Sci. Rep.*, 2012, **2**, 837.
45. Y. Lu, J. Zhao, R. Zhang, Y. Liu, D. Liu, E. M. Goldys, X. Yang, P. Xi, A. Sunna, J. Lu, Y. Shi, R. C. Leif, Y. Huo, J. Shen, J. A. Piper, J. P. Robinson and D. Jin, *Nat. Photonics*, 2014, **8**, 32-36.
46. J. R. Lakowicz, *Principles of Fluorescence Spectroscopy*, 2007, Springer.
47. W. Becker, *J. Microsc.*, 2012, **247**, 119-136.
48. J. Dragavon, M. Amiri, B. Marteyn, P. Sansonetti and S. Shorte, Fluorescence lifetime imaging to quantify sub-cellular oxygen measurements in live macrophage during bacterial invasion, Proc. SPIE 7910, 2011.
49. F. R. Svensson, M. Abrahamsson, N. Strömberg, A. G. Ewing and P. Lincoln, *J. Phys. Chem. Lett.*, 2011, **2**, 397-401.
50. W. Becker, B. Su, A. Bergmann, K. Weisshart and O. Holub, Simultaneous fluorescence and phosphorescence lifetime imaging, Proc. SPIE 7903, 2011.
51. E. P. Buurman, R. Sanders, A. Draaijer, H. C. Gerritsen, J. J. F. van Veen, P. M. Houpt and Y. K. Levine, *Scanning*, 1992, **14**, 155-159.
52. E. Baggaley, S. W. Botchway, J. W. Haycock, H. Morris, I. V. Sazanovich, J. A. G. Williams and J. A. Weinstein, *Chem. Sci.*, 2014, **5**, 879-886.
53. V. K. Ramshesh and J. J. Lemasters, *J. Biomed. Opt.*, 2008, **13**, 064001.
54. J. W. Walton, A. Bourdolle, S. J. Butler, M. Soulie, M. Delbianco, B. K. McMahon, R. Pal, H. Puschmann, J. M. Zwier, L. Lamarque, O. Maury, C. Andraud and D. Parker, *Chem. Commun.*, 2013, **49**, 1600-1602.
55. V. Placide, D. Pitrat, A. Grichine, A. Duperray, C. Andraud and O. Maury, *Tetrahedron Lett.*, 2014, **55**, 1357-1361.
56. S. J. Butler, L. Lamarque, R. Pal and D. Parker, *Chem. Sci.*, 2014, **5**, 1750-1756.
57. A. S. Chauvin, F. Gumy, D. Imbert and J. C. G. Bünzli, *Spectrosc. Lett.*, 2004, **37**, 517-532.
58. X. Peng, F. Song, E. Lu, Y. Wang, W. Zhou, J. Fan and Y. Gao, *J. Am. Chem. Soc.*, 2005, **127**, 4170-4171.
59. R. Horobin, J. Stockert and F. Rashid-Doubell, *Histochem. Cell Biol.*, 2006, **126**, 165-175.
60. A. Foucault-Collet, K. A. Gogick, K. A. White, S. Villette, A. Pallier, G. Collet, C. Kieda, T. Li, S. J. Geib, N. L. Rosi and S. Petoud, *Proc. Natl. Acad. Sci. U.S.A.*, 2013, **110**, 17199-17204.
61. M. Piotto, M. Bourdonneau, K. Elbayed, J.-M. Wieruszeski and G. Lippens, *Magn. Reson. Chem.*, 2006, **44**, 943-947.
62. P.-A. Bouit, G. Wetzel, G. Berginc, B. Loiseaux, L. Toupet, P. Feneyrou, Y. Bretonnière, K. Kamada, O. Maury and C. Andraud, *Chem. Mater.*, 2007, **19**, 5325-5335.